Geophysical Research Letters

Key Points:
- This is the first report on resonant interactions between whistler mode waves in the Earth's magnetosphere
- Two antipropagating whistler mode waves are nonlinearly coupled with each other to generate higher-frequency whistlers
- Excited upper band wave has the same propagating direction as the lower band wave with the relatively higher frequency and has a larger WNA

Correspondence to:
Q. Lu,
qmlu@ustc.edu.cn

First report of resonant interactions between whistler mode waves in the Earth's magnetosphere

Xinliang Gao[1,2] (iD), Quanming Lu[1,2] (iD), and Shui Wang[1,2]

[1]CAS Key Laboratory of Geospace Environment, Department of Geophysics and Planetary Science, University of Science and Technology of China, Hefei, China, [2]Collaborative Innovation Center of Astronautical Science and Technology, Harbin, China

Abstract Nonlinear physics related to whistler mode waves in the Earth's magnetosphere are now becoming a hot topic. In this letter, based on Time History of Events and Macroscale Interactions during Substorms waveform data, we report several interesting whistler mode wave events, where the upper band whistler mode waves are believed to be generated through the nonlinear wave-wave coupling between two lower band waves. This is the first report on resonant interactions between whistler mode waves in the Earth's magnetosphere. In these events, the two lower band whistler mode waves are observed to have oppositely propagating directions, while the generated upper band wave has the same propagating direction as the lower band wave with the relatively higher frequency. Moreover, the wave normal angle of the excited upper band wave is usually larger than those of two lower band whistler mode waves. Our results reveal the large diversity of the evolution of whistler mode waves in the Earth's magnetosphere.

1. Introduction

Whistler mode waves are very intense electromagnetic emissions in the Earth's magnetosphere, which are well known due to their significant role in controlling electron dynamics in the Van Allen radiation belt [*Thorne et al.*, 2010, 2013; *Reeves et al.*, 2013]. Over the past 50 years, whistler mode waves have been thoroughly studied in the linear or quasi-linear frame, and a lot of valuable research results have been achieved. Based on linear and quasi-linear theoretical models, whistler mode waves have been identified as a primary contributor of relativistic electrons in the heart of Van Allen radiation belt [*Reeves et al.*, 2013; *Thorne et al.*, 2013] and a dominant cause of diffuse aurora precipitation into the Earth's atmosphere [*Thorne et al.*, 2010; *Nishimura et al.*, 2013]. However, nonlinear physics related to whistler mode waves in the Earth's magnetosphere are now attracting more and more attention in the community. Many nonlinear phenomena of whistler mode waves, such as the frequency chirping, power gap at about $0.5f_{ce}$, and time domain structures (TDS), have already been widely reported. Whistler mode waves are usually observed with a frequency chirping in the time-frequency spectrogram [*Tsurutani and Smith*, 1974; *Santolik et al.*, 2003; *Li et al.*, 2012], which are commonly believed to be caused by the nonlinear interaction between resonant electrons and whistler mode waves [*Omura et al.*, 2009; *Gao et al.*, 2014]. The upper band whistler mode waves, separated by a power gap around $0.5f_{ce}$ (f_{ce} is the equatorial electron gyrofrequency) from the lower band waves [*Burtis and Helliwell*, 1969; *Li et al.*, 2012], are potentially generated through the nonlinear coupling between the fluctuating electromagnetic fields and densities of nonparallel lower band waves [*Gao et al.*, 2016, 2017]. Besides, the parametric decay of whistler mode waves [*Ke et al.*, 2017] is considered as a potential mechanism to form TDS in the inner magnetosphere [*Agapitov et al.*, 2015]. In this letter, we will report several whistler mode wave events recorded by Time History of Events and Macroscale Interactions during Substorms (THEMIS) waveform data, where two oppositely propagating lower-frequency whistler mode waves are found to be coupled with each other, generating a higher-frequency whistler mode wave. So far, this is the first evidence for the resonant interaction between whistler mode waves in the Earth's magnetosphere.

2. THEMIS Data Analysis

The Time History of Events and Macroscale Interactions During Substorms (THEMIS) spacecraft [*Angelopoulos*, 2008], employing five identically-instrumented probes, are carefully located in a near-equatorial orbit around the Earth. Three inner probes (THEMIS A, D, and E) perfectly cover the main source region of whistler mode waves in the inner magnetosphere, which can provide waveform data with a sampling frequency of ~16 kHz. Each waveform data will last 6–8 s, which are obtained from simultaneous measurements of Search-Coil
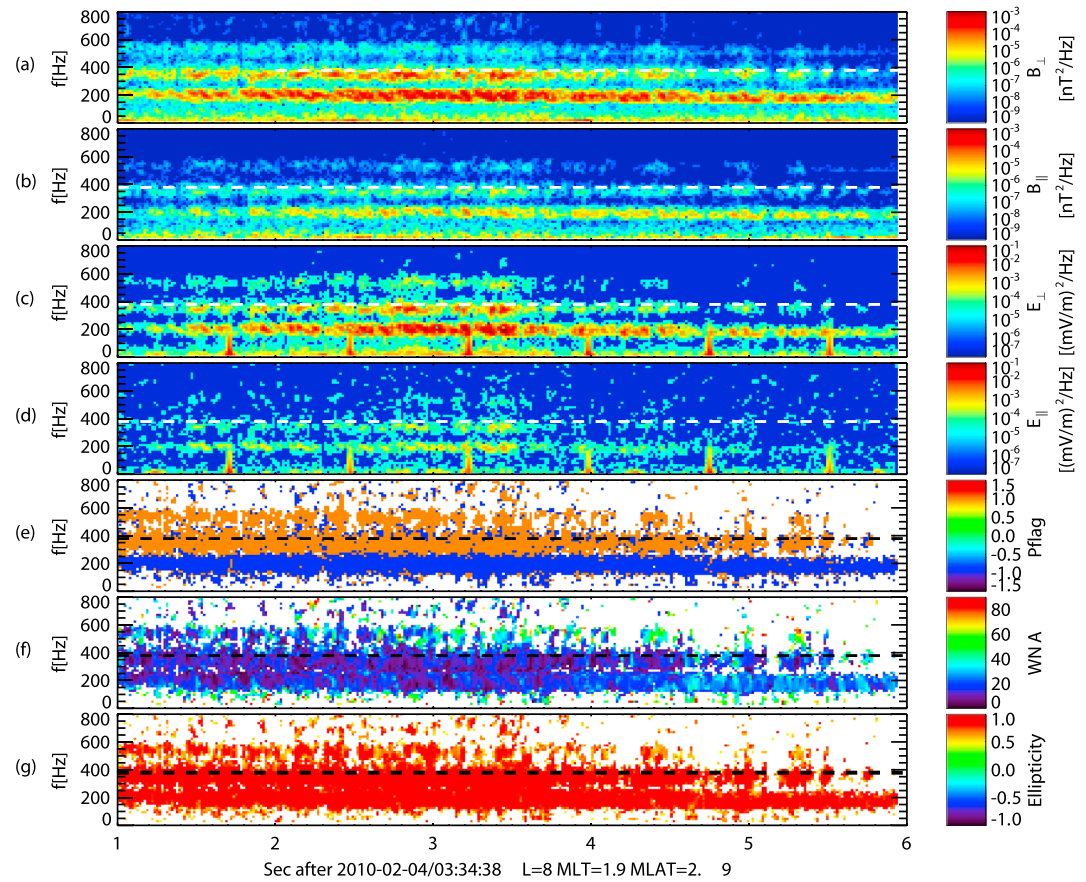
Figure 1. Time evolution of (a–d) the spectrogram of magnetic ($B_\perp$ and $B_{||}$) and electric ($E_\perp$ and $E_{||}$) fields, respectively; (e) a flag, i.e., "Pflag," showing the wave propagating direction, (f) the wave normal angle (WNA), and (g) the ellipticity. In all panels, the dashed horizontal lines in white or black represent $0.5f_{ce}$.

Magnetometer [*Roux et al.*, 2008] and Electric Field Instrument [*Bonnell et al.*, 2008]. Following the same procedure developed by *Bortnik et al.* [2007], the polarization parameters (such as wave normal angle (WNA) and ellipticity) of whistler mode waves are obtained by analyzing waveform data in the field-aligned coordinate system, where the *z* axis is along the background magnetic field. The background magnetic field data are available for nearly all the time, which is measured by the Fluxgate Magnetometer [*Auster et al.*, 2008].

3. Observational Results

Figure 1 shows the overview of a selected whistler mode wave event, which is detected by THEMIS D at L = 8 R_E, magnetic latitude (MLAT) = 2.9°, and magnetic local time (MLT) = 1.9 h. Figures 1a–1d exhibit the dynamic spectrogram for magnetic ($B_\perp$ and $B_{||}$) and electric ($E_\perp$ and $E_{||}$) fields, respectively. The propagating direction (Pflag) of whistler mode waves is shown in Figure 1e, which is determined by both the radial component of the background magnetic field and direction of the Poynting vector [*Li et al.*, 2013]. Here Pflag = 1 means propagating direction away from the magnetic equator, while Pflag = −1 means propagating direction toward the magnetic equator. The wave normal angle (WNA) and ellipticity are shown in Figures 1f and 1g, respectively. Note that the wave normal angle has already been converted to values smaller than 90° to avoid the inherent 180° ambiguity introduced by the calculation method [*Bortnik et al.*, 2007]. The whistler mode waves are typically right-hand polarized, which is consistent with the large ellipticity (>0.9) in Figure 1g. As shown in the dynamic spectrogram (Figures 1a–1d), there are three distinct frequency bands: two belong to lower band waves and one belongs to upper band waves. Moreover, the two lower band waves have opposite propagating directions (Figure 1e) and small wave normal angles (Figure 1f), while the upper band wave has the
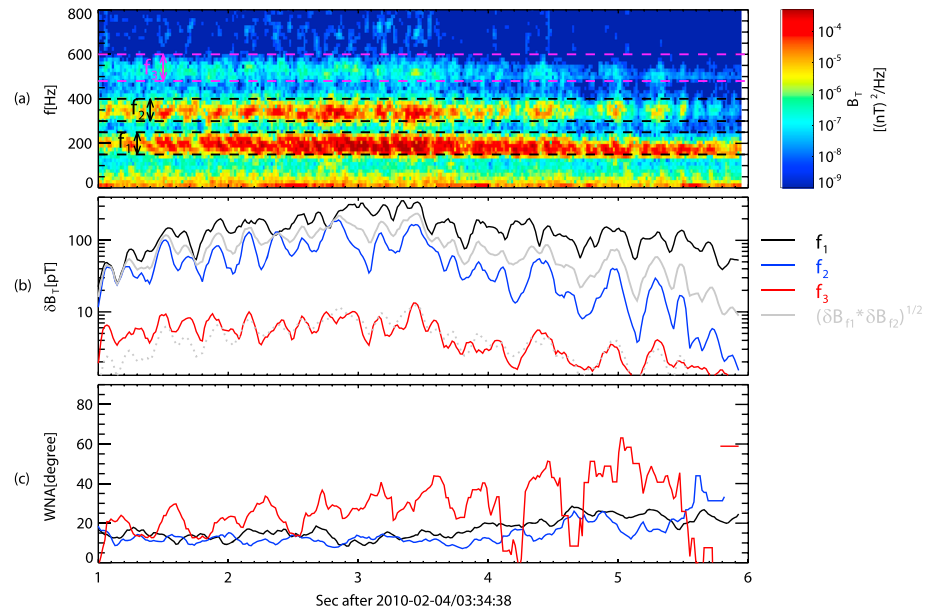
Figure 2. Time evolution of (a) the spectrogram of magnetic fields (B_T), (b) magnetic amplitudes, and (c) the average wave normal angle. In Figures 2b and 2c, f_1, f_2, and f_3 are denoted by black, blue, and red lines, respectively. In Figure 2b, the gray solid line represents an effective amplitude $\sqrt{\delta B_{f1} \delta B_{f2}}$. The gray dotted line denotes the value of $\sqrt{\delta B_{f1} \delta B_{f2}}/20$ as a reference.

same propagating direction as that of the relatively higher-frequency lower band wave (Figure 1e) and larger wave normal angles (Figure 1f).

The upper band whistler mode wave is considered to be excited due to the nonlinear coupling between two lower band waves. Figure 2 provides some quantitative comparisons among three whistler mode waves, which shows (a) the dynamic spectrogram for magnetic fields, and temporal profiles of (b) magnetic amplitude and (c) wave normal angle (WNA). For convenience, we visually classify these whistler mode waves into three separated bands, named as f_1, f_2, and f_3, respectively: 150 Hz $\leq f_1 \leq$ 250 Hz, 300 Hz $\leq f_2 \leq$ 400 Hz, and 480 Hz $\leq f_3 \leq$ 600 Hz. For each band, the magnetic amplitude is calculated by integrating magnetic power from $f_p - 16$ Hz to $f_p + 16$ Hz (f_p is the peak frequency with the dominant power for each band) at each time, while the wave normal angle is the average one from $f_p - 16$ Hz to $f_p + 16$ Hz weighted by the magnetic power. Here we also show an effective amplitude $\sqrt{\delta B_{f1} \delta B_{f2}}$ (δB_{f1} and δB_{f2} are magnetic amplitudes for f_1 and f_2, respectively) in Figure 2b, which is considered to be qualitatively proportional to the nonlinear driven force of the wave-wave coupling between f_1 and f_2. Although the temporal profile of $\sqrt{\delta B_{f1} \delta B_{f2}}$ is similar to that for f_1 or f_2, we can still find that the amplitude of f_3 is well correlated with this effective amplitude. First, the peak amplitude of f_3 just corresponds to the peak effective amplitude at about 3.5 s, rather than the peak amplitude of f_1 or f_2. Second, the ratio between the effective amplitude and that of f_3 seems to be a constant during this event, which is estimated as ~20 as shown in Figure 2b. Finally, the wave band f_3 can be still observed even the amplitude of f_2 down to below 10 pT after 5.5 s, which may be due to the compensation of the large amplitude of f_1. As shown in Figure 2c, for f_1 and f_2, their wave normal angles are quite small and nearly remain below 20°, while the wave normal angle of f_3 is much larger, which can even reach about 60° at some time.

The bicoherence analysis is a useful method to check the phase coupling among three wave modes [*van Milligen et al.*, 1995; *Agapitov et al.*, 2015; *Gao et al.*, 2016, 2017], and the large bicoherence index (close to 1) means that these signals are involved in a strong wave-wave coupling process. We arbitrarily extract one perpendicular component (E_y) and parallel component (E_z) of electric fields from waveform data for a 70 ms interval to calculate the bicoherence index, which is given by $\left| \left\langle E_z(f_1) E_y(f_2) E_y^*(f_3) \right\rangle \right|^2 / \left\langle \left| E_z(f_1) E_y(f_2) \right|^2 \right\rangle \left\langle \left| E_y^*(f_3) \right|^2 \right\rangle$ (where $f_3 = f_1 + f_2$ and the bracket $\langle \rangle$ denotes an average over the 70 ms
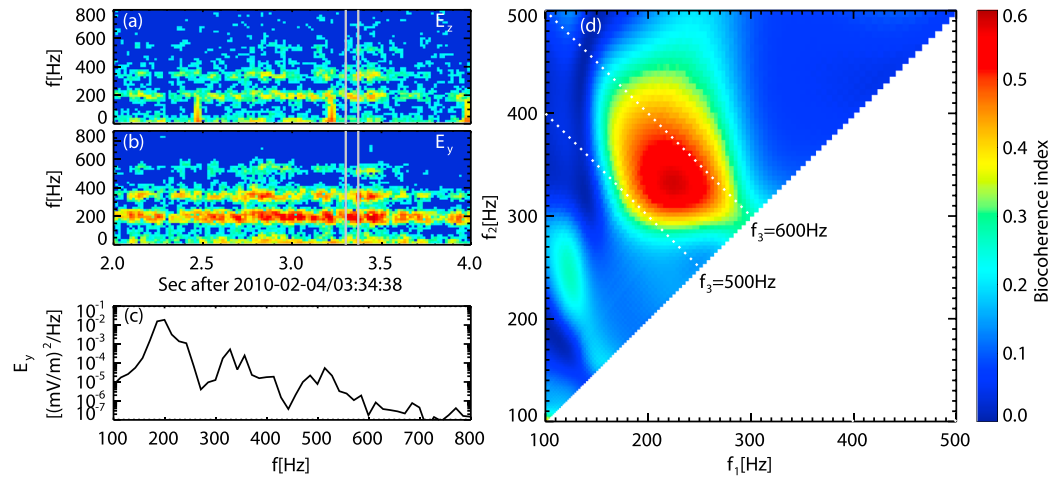
Figure 3. (a and b) Time evolution of the spectrogram for E_z and E_y, respectively; (c) the power spectrum of E_y obtained from the Fourier transform for the selected interval marked by gray lines in Figures 3a and 3b, and (d) the distribution of the bicoherence index where f_2 is larger than f_1. In Figure 3d, as a reference, the white dotted lines mark $f_3 = f_1 + f_2 = 500$ Hz and 600 Hz.

interval). Figures 3a and 3b show the dynamic spectrogram for E_z and E_y, respectively, while Figure 3c illustrates the spectrum of E_y obtained from the Fourier transform for the selected interval marked by gray lines in Figures 3a and 3b. Figure 3d gives the distribution of the bicoherence index where f_2 is larger than f_1. It is worth noting that the large bicoherence index shown in Figure 3d indicates that the three wave modes satisfy the resonant condition, i.e., $f_3 = f_1 + f_2$. We can easily find that the large bicoherence index occurs in the region with 180 Hz $< f_1 <$ 270 Hz and 300 Hz $< f_2 <$ 400 Hz (i.e., 480 Hz $< f_3 <$ 670 Hz), whose maximum value can reach up to about 0.6 at $f_3 \approx 550$ Hz. Moreover, this frequency region is quite consistent with the spectrum shown in Figure 3b, supporting that f_3 should be generated due to the resonant interaction between f_1 and f_2.

In this study, we also consider the resonant condition of wave numbers among three wave modes. Since this event occurs quite near the magnetic equator (MLAT = 2.9°), so we assume that two lower band waves (f_1 and f_2) are just linearly excited and very close to their source regions, meaning they approximately satisfy the linear dispersion relation. From Figures 2 and 3, we extract a set of parameters at about 3.3 s: $f_1 = 200$ Hz, $f_2 = 320$ Hz, $\theta_1 = \theta_2 = 15°$, $B_0 = 27.5$ nT, and $n_e = 1.5$ cm^{-3}. Here the electron density n_e is inferred from the spacecraft potential and the electron thermal speed [*Li et al.*, 2010]. And the wave numbers of f_1 and f_2 are estimated based on the linear dispersion relation in a cold plasma, which is given as [*Verkhoglyadova et al.*, 2010; *Mourenas et al.*, 2015]

$$\frac{k^2 c^2}{4\pi^2 f^2} = 1 + \frac{\omega_{pe}^2}{4\pi^2 f(f_{ce} \cos\theta - f)}$$

where ω_{pe}, k, and θ are the plasma frequency, wave number, and wave normal angle, respectively. Then, we can obtain the wave numbers of f_1 and f_2 as $k_1 c/\omega_{pe}$=0.61 and $k_2 c/\omega_{pe}$=0.87, respectively. Figure 4 schematically shows the distribution of wave vectors for three wave modes in two cases. In both panels, the plane is determined by the wave vector $\mathbf{k_1}$, and it is lying in the second quadrant due to its antiparallel propagating direction (Figure 1). The parallel component of $\mathbf{k_2}$ can also be determined along the background magnetic field, while its perpendicular component may freely rotate in the plane perpendicular to the background magnetic field. Here we only choose two extreme cases: (a) the perpendicular components of $\mathbf{k_1}$ and $\mathbf{k_2}$ are in the same direction, then f_3 will get the maximum theoretical wave normal angle, and (b) the perpendicular components of $\mathbf{k_1}$ and $\mathbf{k_2}$ are in the opposite directions, then f_3 will get the minimum theoretical wave normal angle. Based on the resonant condition of wave numbers, i.e.,$\mathbf{k_3} = \mathbf{k_1} + \mathbf{k_2}$, the maximum and minimum theoretical wave normal angles of f_3 are calculated as 57° and 15°, respectively. The observed wave normal angle of f_3 is about 40° (Figure 2c), which just falls within the above theoretical range [15°, 57°]. Moreover, there are two points in Figure 4 especially worthy of notice. First, the propagating direction of f_3
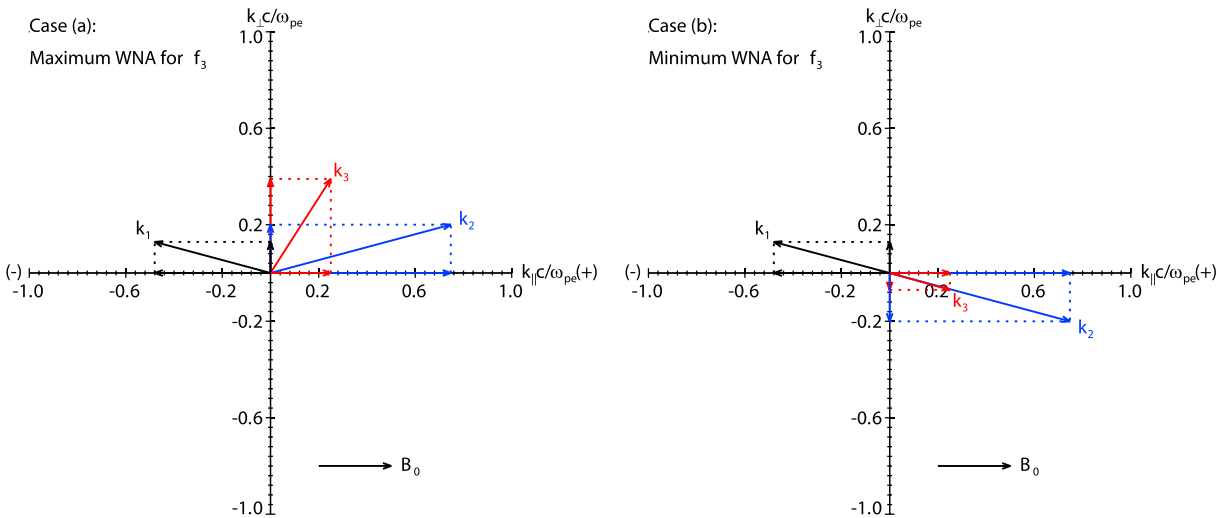
Figure 4. The distribution of wave vectors for three wave modes in two cases: (a) f_3 gets its maximum wave normal angle and (b) f_3 gets its minimum wave normal angle. In both panels, the plane is determined by the wave vector $\mathbf{k_1}$. The wave vectors of f_1, f_2, and f_3 are denoted by black, blue, and red arrows, respectively. Here the wave vector $\mathbf{k_3}$ is given by $\mathbf{k_1} + \mathbf{k_2}$.

should be same as that of f_2, since f_2 typically has a larger parallel wave number than f_1. Second, just as discussed above, the excited wave mode f_3 tends to have a larger wave normal angle.

So far, we have identified six whistler mode events recorded by THEMIS probes, where the higher-frequency wave is considered to be excited through the nonlinear wave-wave coupling between two lower-frequency waves. All the events, including the one analyzed above, are listed in Table 1, and they are found to have several common properties. All the events occur at relatively larger L shells (L > 8), where the background magnetic field is very weak. This may be for the reason that the weak background magnetic field makes the amplitude threshold of the nonlinear wave-wave coupling more easily satisfied. The two lower frequency whistler mode waves (f_1 and f_2) are observed to have opposite propagating directions, while the higher-frequency wave (f_3) has the same propagating direction as f_2. Moreover, the higher-frequency wave (f_3) typically has larger wave normal angles than that of f_1 or f_2 (not shown here).

4. Conclusions and Discussion

In this letter, with THEMIS waveform data, we report several interesting whistler mode wave events, where the upper band whistler mode waves are believed to be generated through the nonlinear wave-wave coupling between two lower band waves. This is the first observational evidence for resonant interactions between whistler mode waves in the Earth's magnetosphere. In these events, the two lower band whistler mode waves are found to have opposite propagating directions, while the generated upper band wave has the same propagating direction as the relatively higher-frequency lower band wave. Moreover, the wave normal angle of the excited upper band wave is usually larger than those of two lower band whistler mode waves.

Table 1. Parameters of All Selected Whistler Mode Wave Events

Event No.	Time	L Shell	MLT	MLAT	f_1, f_2, f_3 (Hz)
1	15-11-2008/19:09:01–09	11.1	8.3	−5.6	250(−), 650(+), 900(+)[a]
2	4-2-2010/03:34:38–44	8.0	1.9	2.9	200(−), 320(+), 520(+)
3	12-3-2014/14:35:29–37	10.9	12.8	2.4	200(−), 350(+), 550(+)
4	6-7-2014/00:22:51–59	9.9	4.8	−9.8	140(+), 260(−), 400(−)
5	6-7-2014/00:23:00–07	9.9	4.8	−9.8	140(+), 260(−), 400(−)
6	1-4-2015/06:30:52–59	11.8	14.7	−1.2	350(+), 550(−), 900(−)

[a]Here the plus sign or minus sign denotes that the propagating direction of whistler waves is away from or toward the magnetic equator, respectively.

In these whistler mode wave events, the magnetic amplitudes of two lower band mode waves are quite comparable (Figure 2b), but their propagating directions are just opposite. Therefore, we assume that two lower band whistler mode waves are initially generated from two different source regions, and then meet with each other during their propagation at somewhere between two source regions. Since the main source region of whistler mode waves is near the magnetic equator, the whistler mode events discussed here are more easily detected in the low-latitude region (Table 1). If two lower band waves from different source regions have the same propagating direction, they should meet with each other in relatively higher-latitude regions because it will take long time for the relatively higher-frequency wave to catch up the other wave mode. Unfortunately, both THEMIS and Van Allen Probes are just located in a near-equatorial orbit, so we still require the high-latitude waveform data to verify this scenario.

Here we assume that the two pump whistler mode waves (f_1 and f_2) are linearly excited due to anisotropic hot electrons and very close to their source regions; therefore, they are the eigenmodes in the plasma system and approximately satisfy the linear dispersion relation. While, the upper band whistler mode wave f_3 is excited due to the nonlinear coupling between two pump waves, which is supported by the phase-locked condition among three wave modes shown in Figure 3d. This phase-locked condition among three wave modes means $f_3 = f_1 + f_2$ and $\mathbf{k_3} = \mathbf{k_1} + \mathbf{k_2}$ [$Lagoutte\ et\ al.$, 1989]. In this nonlinear framework, this excited wave mode is a driven mode, but not necessary an eigenmode of the plasma system; i.e., it may not satisfy the linear dispersion relation. However, both theoretical and simulation studies are still required to exhibit the detailed physical process, but it is beyond the scope of this paper.

During the propagation of whistler mode waves in the Earth's magnetosphere, besides the damping and reflection predicted by the linear theory, they may also experience some nonlinear physical processes, such as lower band cascade [$Gao\ et\ al.$, 2016, 2017] and parametric decay [$Agapitov\ et\ al.$, 2015; $Ke\ et\ al.$, 2017]. Our study further points out that whistler mode waves in the magnetosphere can be nonlinearly coupled with each other. This implies that the nonlinear physical phenomena related to whistler mode waves are quite common, and we should take both linear and nonlinear effects into consideration when modeling the evolution of whistler mode waves in the Earth's magnetosphere. Moreover, our results may also provide a potential mechanism to excite upper band whistler mode waves, especially oblique whistler mode waves.

References

Agapitov, O. V., V. Krasnoselskikh, F. S. Mozer, A. V. Artemyev, and A. S. Volokitin (2015), Generation of nonlinear electric field bursts in the outer radiation belt through the parametric decay of whistler waves, $Geophys.\ Res.\ Lett.$, 42, 3715–3722, doi:10.1002/2015GL064145.
Angelopoulos, V. (2008), The THEMIS mission, $Space\ Sci.\ Rev.$, 141, 5–34.
Auster, H. U., et al. (2008), The THEMIS fluxgate magnetometer, $Space\ Sci.\ Rev.$, 141, 235–264, doi:10.1007/s11214-008-9365-9.
Bonnell, J. W., F. S. Mozer, G. T. Delory, A. J. Hull, R. E. Ergun, C. M. Cully, V. Angelopoulos, and P. R. Harvey (2008), The Electric Field Instrument (EFI) for THEMIS, $Space\ Sci.\ Rev.$, 141, 303–341, doi:10.1007/s11214-008-9469-2.
Burtis, W. J., and R. A. Helliwell (1969), Banded chorus—A new type of VLF radiation observed in the magnetosphere by OGO 1 and OGO 3, $J.\ Geophys.\ Res.$, 74, 3002, doi:10.1029/JA074i011p03002.
Bortnik, J., J. W. Cutler, C. Dunson, and T. E. Bleier (2007), An automatic wave detection algorithm applied to Pc1 pulsations, $J.\ Geophys.\ Res.$, 112, A04204, doi:10.1029/2006JA011900.
Gao, X. L., W. Li, R. M. Thorne, J. Bortnik, V. Angelopoulos, Q. M. Lu, X. Tao, and S. Wang (2014), New evidence for generation mechanisms of discrete and hiss-like whistler mode waves, $Geophys.\ Res.\ Lett.$, 41, 4905–4811, doi:10.1002/2014GL060707.
Gao, X. L., Q. M. Lu, J. Bortnik, W. Li, L. J. Chen, and S. Wang (2016), Generation of multi-band chorus by lower band cascade in the Earth's magnetosphere, $Geophys.\ Res.\ Lett.$, 43, 2343–2350, doi:10.1002/2016GL068313.
Gao, X. L., Y. G. Ke, Q. M. Lu, L. J. Chen, and S. Wang (2017), Generation of multiband chorus in the Earth's magnetosphere: 1-D PIC simulation, $Geophys.\ Res.\ Lett.$, 44, 618–624, doi:10.1002/2016GL072251.
Ke, Y. G., X. L. Gao, Q. M. Lu, and S. Wang (2017), Parametric decay of a parallel propagating monochromatic whistler wave: Particle-in-cell simulations, $Phys.\ Plasmas$, 24, 012108.
Lagoutte, D., F. Lefeuvre, and J. Hanasz (1989), Application of bicoherence analysis in study of wave interactions in space plasma, $J.\ Geophys.\ Res.$, 94, 435–442, doi:10.1029/JA094iA01p00435.
Li, W., R. M. Thorne, J. Bortnik, Y. Nishimura, V. Angelopoulos, L. Chen, J. P. McFadden, and J. W. Bonnell (2010), Global distributions of suprathermals electrons observed on THEMIS and potential mechanisms for access into the plasmasphere, $J.\ Geophys.\ Res.$, 115, A00J10, doi:10.1029/2010JA015687.
Li, W., R. M. Thorne, J. Bortnik, X. Tao, and V. Angelopoulos (2012), Characteristics of hiss-like and discrete whistler-mode emissions, $Geophys.\ Res.\ Lett.$, 39, L18106, doi:10.1029/2012GL053206.
Li, W., J. Bortnik, R. M. Thorne, C. M. Cully, L. Chen, V. Angelopoulos, Y. Nishimura, J. B. Tao, J. W. Bonnell, and O. LeContel (2013), Characteristic of the Poynting flux and wave normal vectors of whistler-mode waves observed on THEMIS, $J.\ Geophys.\ Res.\ Space\ Physics$, 118, 1461–1471, doi:10.1002/jgra.50176.
Mourenas, D., A. V. Artemyev, O. V. Agapitov, V. Krasnoselskikh, and F. S. Mozer (2015), Very oblique whistler generation by low-energy electron streams, $J.\ Geophys.\ Res.\ Space\ Physics$, 120, 3665–3683, doi:10.1002/2015JA021135.

Nishimura, Y., et al. (2013), Structures of dayside whistler-mode waves deduced from conjugate diffuse aurora, *J. Geophys. Res. Space Physics*, *118*, 664–673, doi:10.1029/2012JA018242.

Omura, Y., M. Hikishima, Y. Katoh, D. Summers, and S. Yagitani (2009), Nonlinear mechanisms of lower-band and upper-band VLF chorus emissions in the magnetosphere, *J. Geophys. Res.*, *114*, A07217, doi:10.1029/2009JA014206.

Reeves, G. D., et al. (2013), Electron acceleration in the heart of the Van Allen radiation belts, *Science*, *341*, 991.

Roux, A., O. Le Contel, C. Coillot, A. Bouabdellah, B. de la Porte, D. Alison, S. Ruocco, and M. C. Vassal (2008), The search coil magnetometer for THEMIS, *Space Sci. Rev.*, *141*(1–4), 265–275, doi:10.1007/s11214-008-9455-8.

Santolik, O., D. A. Gurnett, and J. S. Pickett (2003), Spatio-temporal structure of storm-time chorus, *J. Geophys. Res.*, *108*(A7), 1287, doi:10.1029/2002JA009791.

Thorne, R. M., B. Ni, X. Tao, R. B. Horne, and N. P. Meredith (2010), Scattering by chorus waves as the dominant cause of diffuse auroral precipitation, *Nature*, *467*, 943.

Thorne, R. M., et al. (2013), Rapid local acceleration of relativistic radiation-belt electrons by magnetospheric chorus, *Nature*, *504*, 411.

Tsurutani, B. T., and E. J. Smith (1974), Postmidnight chorus: A substorm phenomenon, *J. Geophys. Res.*, *79*, 118, doi:10.1029/JA079i001p00118.

van Milligen, B. P., E. Sanchez, T. Estrada, C. Hidalgo, B. Branas, B. Carreras, and L. Garcia (1995), Wavelet bicoherence: A new turbulence analysis tool, *Phys. Plasmas*, *2*, 3017.

Verkhoglyadova, O. P., B. T. Tsurutani, and G. S. Lakhina (2010), Properties of obliquely propagating chorus, *J. Geophys. Res.*, *115*, A00F19, doi:10.1029/2009JA014809.